

Coordination nanosheets stabilizing efficient tin-based perovskite solar cells

Dhruba B. Khadka^{1,§,*}, Yan-Chen Kuo², Yi Zhen Li², Muhammad Waqas², You-Jia Xu², Masatoshi Yanagida¹, Hiroshi Nishihara³, Kazuhito Tsukagoshi⁴, Mitch Ming-Chi Chou^{2,5}, Yasuhiro Shirai¹, and Ying-Chiao Wang^{2,§,*}

¹Photovoltaic Materials Group, Center for GREEN Research on Energy and Environmental Materials, National Institute for Materials Science (NIMS), 1-1 Namiki, Tsukuba, Ibaraki 305-0044, Japan

²Department of Materials and Optoelectronic Science, National Sun Yat-sen University, Kaohsiung, 804, Taiwan, R.O.C.

³Research Institute for Science and Technology, Tokyo University of Science, 2641 Yamazaki, Noda, Chiba 278-8510, Japan

⁴WPI International Center for Materials Nanoarchitectonics (WPI-MANA), National Institute for Materials Science (NIMS), 1-1 Namiki, Tsukuba, Ibaraki 305-0044, Japan

⁵Program on Key Materials, Academy of Innovative Semiconductor and Sustainable Manufacturing, National Cheng Kung University, Tainan, 70101, Taiwan, R.O.C.

[§]D. B K. and Y.-C.W. contributed equally to this work.

*Correspondence and requests for materials should be addressed to D. B. K. (email: KHADKA.B.Dhruba@nims.go.jp) and Y.-C. Wang (email: ycwang@mail.nsysu.edu.tw)

ABSTRACT

Tin-based perovskites, characterized by their advantageous bandgap and much lower toxicity, have emerged as a promising alternative to lead-based perovskites in solar cell applications. However, the efficiency and stability of tin-based perovskite solar cells (Sn-PSCs) are still limited by defects resulting from the easy oxidation of Sn^{2+} to Sn^{4+} . Herein, an approach to enhance the optoelectronic performance of Sn-PSCs by incorporating terpyridine-zinc(II) (ZnTPY) coordination nanosheets (CONASHs), synthesized via liquid-liquid interfacial polymerization, into tin-based perovskites is delivered. Following physical fragmentation, ZnTPY CONASHs, enriched with unsaturated terpyridine groups, undergo multidentate chelation with SnI_2 , forming ZnTPY: SnI_2 heterogeneous nuclei. This process effectively enhances the crystallization of tin-based perovskites while mitigating recombination and defect chemistry related to Sn^{2+} oxidation. As a result of superior crystal quality, the ZnTPY CONASH-modified tin perovskite exhibits a longer photoluminescence lifetime. Consequently, the Sn-PSC incorporating ZnTPY complex achieves a power conversion efficiency of 11.59%, compared to 9.14% for the control device, along with improved operational stability without encapsulation. Thus, this work underscores the critical role of coordination nanosheets for regulating coordination in the precursor solution to achieve high-quality tin-based perovskite films, offering a pathway to more efficient and stable Sn-PSCs.

Keywords: Tin perovskite; coordination nanosheet, crystallization; oxidation; additive

Introduction

Lead-incorporated halide perovskite crystals have made significant advancements within the photovoltaic community, leading to an increase in the power conversion efficiency (PCE) of perovskite solar cells (PSCs) to over 26% in the past decade.¹⁻⁴ However, the well-established environmental and human health risks linked to lead pose a substantial barrier to the commercialization of these lead-containing photovoltaic technologies.^{5,6} Therefore, several low-toxicity elements, such as copper,⁷ bismuth,⁸ and tin (Sn),⁹ have been explored as potential alternatives to highly toxic lead. Among these candidates, Sn-related PSCs (Sn-PSCs) are recognized as the most suitable substitute for lead PSCs, owing to their ideal bandgaps of 1.2-1.4 eV,⁹ approaching the Shockley-Queisser limit,¹⁰ as well as their high carrier mobility,¹¹ high absorption coefficient,¹² and low exciton binding energy.¹³ However, the PCEs of Sn-based PSCs remain considerably lower than those of lead-based PSCs due to several defect-induced factors.¹⁴ The primary defect in Sn-perovskite crystals arises from the easy oxidation of Sn²⁺ to Sn⁴⁺, which leads to the generation of numerous Sn²⁺ vacancies.^{15,16} These point defects induce p-type doping, creating multiple trap-state densities that ultimately reduce carrier diffusion lengths.¹⁷ Additionally, the rapid crystallization of SnI₂ with organic ammonium ions complicates the control of film morphology during solution processing,¹⁸ resulting in severe non-radiative recombination losses¹⁹ and further limiting the performance of Sn-PSCs.

To address these issues, substantial efforts have been made in recent years. For instance, mixed-organic-cation engineering has been proven to be an effective strategy for modulating crystallization and film morphology in Sn-PSCs.^{20,21} Initially, methylammonium cation (MA⁺) was proposed as the sole organic cation for Sn-PSCs;^{22,23} nevertheless, because of the deficient quality of tin perovskite films, the first-generation devices were unstable and exhibited poor reproducibility.²⁴ Considering this challenge, partially replacing MA⁺ with formamidinium

cation (FA⁺) at the A-site of perovskites would be more advantageous, as the FA⁺ provides better stabilization of the crystal structure compared to MA⁺ in tin-based perovskite crystals.²⁵ This occurs because the larger size of FA⁺ reduces the antibonding coupling of Sn s orbitals with I p orbitals in Sn-PSCs.²⁶⁻²⁸ Thus, the formation energy of tin vacancies in Sn-based perovskite crystals increases. Consequently, the charge carrier type of FA⁺-included tin perovskite can be modified from p-type to intrinsic state, indicating that point defects can be considerably mitigated. While reducing point defects can enhance PCEs of Sn-PSCs, ensuring consistent film quality over time remains a challenge. Water or oxygen molecule adsorption on tin perovskites is commonly recognized as a key factor contributing to crystal decomposition.²⁹ Thus, the incorporation of bulky ammonium cations, such as butylammonium (BA⁺)³⁰ and phenylethylammonium (PEA⁺),³¹ has proven effective in reducing moisture ingress at grain boundaries of Sn-based perovskite films, analogous to their function in lead perovskites.³² These bulky cations facilitate the transformation of tin-based perovskites from the three-dimensional (3D) architecture into numerous two-dimensional (2D) fragments with hydrophobic characteristics, significantly enhancing the stability of Sn-PSCs.³³ However, slicing 3D perovskites into partially 2D pieces relies only on weak monodentate chelation, making it challenging to maintain high crystallinity and thereby limiting device performance. Hence, identifying new additives that interact more strongly with Sn-perovskites could further enhance the crystallinity of 2D/3D perovskites, along with simultaneous gains in both PCE and stability.

Here, π -conjugated terpyridine-zinc(II) (ZnTPY) coordination nanosheets (CONASHs), synthesized via a liquid-liquid interfacial method,^{34,35} were used as multidentate chelators to facilitate heterogeneous nucleation of perovskites, thereby strengthening interactions between additives and PEA⁺-containing Sn-perovskite crystals. It has been observed that the incorporation of ZnTPY CONASHs supports the formation of (10 $\bar{1}$)' planes in perovskites

while concurrently diminishing the prevalence of $(20\bar{2})'$ facets. This implies that the strong chelation between ZnTPY and the perovskites can effectively restrict the formation of 2D perovskites, even in the presence of bulky PEA⁺ ions. Therefore, the crystallization and orientation of Sn-perovskites are improved, yielding stronger antioxidant passivation and a prolonged photoluminescence (PL) lifetime. Resultantly, the ZnTPY-based Sn-PSC exhibited high operational stability, with a meaningful boost in PCE from 9.14% to 11.59%. This work thus presents a novel additive engineering that enables Sn-perovskites to achieve hydrophobicity while preserving high crystallinity, ultimately leading to high-performance PSCs.

Results and discussion

Synthesis and fragmentation of ZnTPY CONASHs

ZnTPY complex is synthesized via a one-step, bottom-up spontaneous coordination reaction between organic ligand molecules and zinc ions at room temperature, as detailed in our previous report,³⁴ resulting in a 2D motif that exhibits the characteristics of metal complexes. The synthesis of CONASH involves the use of a three-way symmetric 1,3,5-tris[4-(4'-2,2':6',2''-terpyridyl)phenyl]-benzene (TPY) as the organic ligand, as illustrated in Figure 1a. Additionally, the Zn(NH₄)₂(SO₄)₂ salt dissociates in water to yield the inorganic zinc source. Following the reaction, ZnTPY features a structure consisting of repeating units arranged as TPY-Zn(II)-(SO₄)²⁻-Zn(II)-TPY. Figure 1b shows an X-ray photoelectron spectroscopy (XPS) image of a ZnTPY nanosheet, which shows a nitrogen signal in the high-resolution N 1s spectrum at 398.6 eV, indicating that the ZnTPY film is enriched with TPY groups. Continuing to explore higher binding energy positions in the XPS spectrum, satellite doublet peaks in the Zn 2p spectrum are observed at 1021.5 and 1044.7 eV, confirming the presence of Zn(II)-N

bonds, as demonstrated in Figure 1c. Therefore, these XPS spectra validate the completion of the coordination reaction between zinc ions and the pyridines of TPY ligands.

In the perovskite precursor solution, we mainly utilized ZnTPY CONASH as an additive for the Sn-perovskite. However, the excellent film-forming ability of the as-synthesized CONASH results in a majority of the reactive TPY groups being coordinated with Zn, which may limit the potential of ZnTPY to enhance the performance of the perovskite. Although bare TPY molecules show a strong chelation effect with the perovskite precursor, they tend to form a gel-like state, which can hinder subsequent solution processing.³⁴ To optimize reactivity, coordinating partial TPY ligands with Zn(II) can effectively prevent excessive reactivity while simultaneously increasing the contact area between the additive and the perovskite precursor through the formation of a 2D structure. Figure 1d provides a detailed description of the synthesis steps for the ZnTPY CONASH material, which is abundant in TPY functional groups. The left panel of Figure 1d illustrates a liquid/liquid biphasic polymerization conducted using dual-layer solutions with differing polarities. Where the upper layer comprises a high-polarity aqueous solution containing $\text{Zn}(\text{NH}_4)_2(\text{SO}_4)_2$ salt and NaBr charge compensator, while the lower layer contains TPY dispersed in the low-polarity solvent dichloromethane (DCM). Upon leaving these two phases undisturbed at room temperature for three days, the initially transparent interface in the reaction vial gradually turned pale yellow (center of Figure 1d). Figures 1b and 1c present XPS spectra that verify the successful formation of ZnTPY CONASHs. After replacing the solvent with dimethylformamide, we applied ultrasonic agitation to fragment ZnTPY, yielding CONASH particles that are rich in uncoordinated TPY edges (as shown in the right side of Figure 1d and the transmission electron microscopy image in Figure S1). Next, these tailored ZnTPY CONASHs were added to the perovskite precursor solution to serve as agents for enhancing performance.

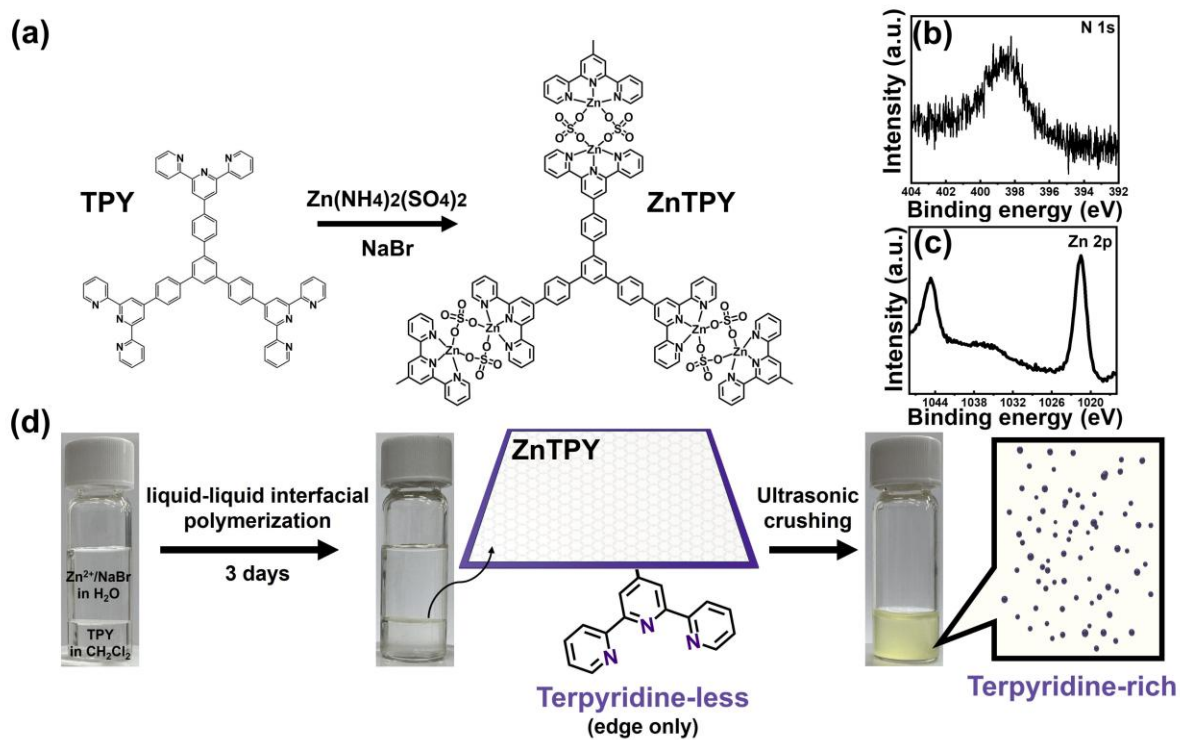


Figure 1. (a) Synthesis pathway of the ZnTPY CONASH. Figures (b) and (c) present the high-resolution XPS spectra of the N 1s and Zn 2p core levels for the as-synthesized ZnTPY CONASHs. Figure (d) illustrates the liquid/liquid interfacial synthesis process, showing the layered liquid/liquid phases, the reaction after 3 days, and the CONASH/DMF suspension following ultrasonic fragmentation.

Verification of ZnTPY:SnI₂ heterogeneous nuclei

The PEA_{0.15}FA_{0.8}MA_{0.05}SnI₃ perovskite photosensitizer used in this study is formed through the reaction of two precursors: organic ammonium iodide and inorganic SnI₂. Initially, the dissociated I⁻ ions from organic ammonium salts react with SnI₂ to form octahedral [SnI₆]⁴⁻ homogeneous nuclei. These octahedral frameworks subsequently grow into a 3D structure, with organic ammonium ions spontaneously occupying the interstitial spaces between octahedra to form a photoactive perovskite crystal. During this process, the formation of [SnI₆]⁴⁻ unit faces a significant energy barrier.^{36,37} When CONASHs are added into the perovskite precursor solution, the uncoordinated TPY sites of incomplete ZnTPY can effectively perform multidentate chelation with SnI₂ to form [(SnI_{6-x})⁴⁻-ZnTPY] (where x represents the number of tin ions coordinated by TPY in the inorganic octahedral structural units within the perovskite crystals) heterogeneous nuclei more readily than I⁻ ions, thereby reducing the crystallization energy barrier of the Sn-perovskite.

To verify the formation of heterogeneous nucleation centers, we analyzed the differences in signals from X-ray diffraction (XRD) spectra of SnI₂ films with and without the addition of ZnTPY. As displayed in Figure 2a, the XRD pattern reveals the hexagonal SnI₂ peak at a diffraction angle of $2\theta \approx 12.3^\circ$, which matches the (001) reflection.³⁸ Compared to the standard sample, the intensity of the (001) diffraction peak in the ZnTPY CONASH-modified films was markedly reduced. This change is ascribed to the easy insertion of CONASH into SnI₂ aggregates via multidentate chelation, which disrupts the hexagonal lattice structure of SnI₂.

Based on the findings mentioned above, we can propose two possible coordination pathways. The chemical structures illustrated in Figure 2c suggest that the first pathway involves a single TPY group coordinating with Sn, while the second pathway involves two adjacent TPY units coordinating simultaneously with a single Sn atom. In both scenarios, ZnTPY serves as the multidentate chelator, and this type of chemical interaction is stronger

than the reaction between Γ^- and Sn. Therefore, this multidentate coordination complex, which presents a low nucleation energy barrier, will replace the conventional $[\text{SnI}_6]^{4-}$ homogeneous nuclei, resulting in the formation of $[(\text{SnI}_{6-x})^{4-}\text{-ZnTPY}]$ heterogeneous nuclei (hereafter referred to as ZnTPY:SnI₂).

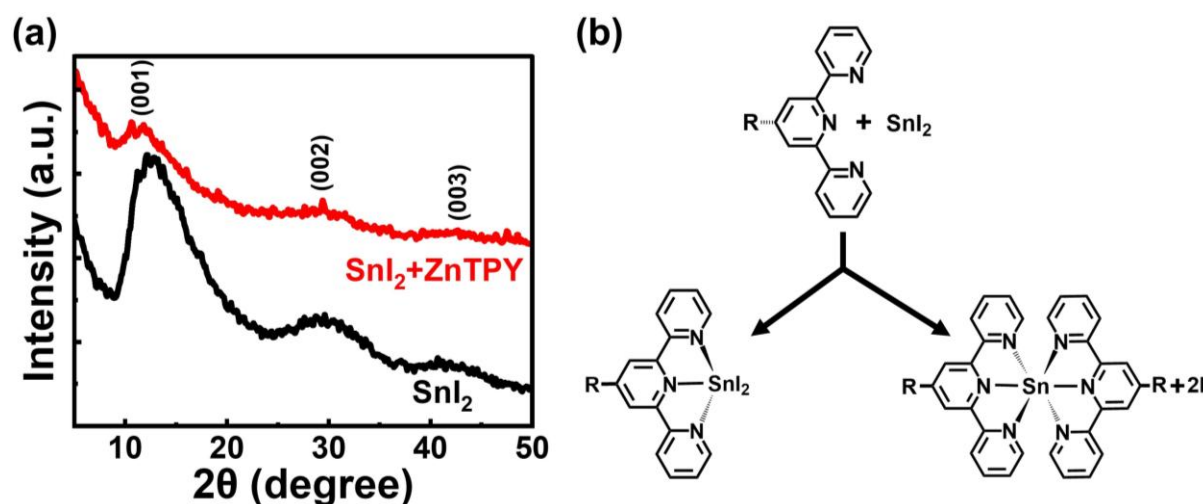


Figure 2. Chelation of SnI₂ with ZnTPY fragment: (a) XRD signals of ZnTPY:SnI₂ and bare SnI₂ films. (b) Two possible mechanisms for the formation of ZnTPY:SnI₂ complexes.

Characterization of Sn-perovskites modified with ZnTPY CONASHs

To investigate the structural changes imparted by the ZnTPY:SnI₂ heterogeneous nuclei on Sn-perovskite crystals, we conducted a detailed analysis using X-ray diffraction (XRD) technique. Herein, ZnTPY CONASHs are dissolved in the PEA⁺-containing perovskite precursor solution at a concentration of 0.075 mg/mL. Subsequently, ZnTPY-seeded PEA_{0.15}FA_{0.8}MA_{0.05}SnI₃ perovskite films are fabricated using an antisolvent spin-coating method (for details, refer to the Experimental Details section). Generally, the introduction of bulk PEA⁺ ions spontaneously cleaves the 3D Sn-perovskite crystals into 2D few-layered components ($n < 5$). If the stoichiometric ratio of PEA⁺ is insufficient, the Sn-perovskite structure develops to its 3D analog, specifically a multi-layered 2D ($n > 5$)/3D hybrid structure. In this scenario, the

structure of the 2D/3D perovskite increasingly approximates a 3D configuration. This indicates that the addition of a small amount of PEA^+ to the Sn-perovskite results in the XRD signal manifesting at an angle comparable to that observed in the 3D structure.³³ From our study, the $(10\bar{1})'$ and $(20\bar{2})'$ facets observed in the quasi-cubic 2D/3D $\text{PEA}_{0.15}\text{FA}_{0.8}\text{MA}_{0.05}\text{SnI}_3$ perovskite exhibit similar angles, with the two peaks differing by approximately 14° and 28° , respectively, when compared to the (100) and (200) planes of the cubic 3D Sn-perovskite crystals,^{39,40} as illustrated in Figure 3a. The addition of PEA^+ caused no significant shifts in the diffraction angles of these two pairs of crystal planes, suggesting that the in-plane lattice parameters along the a and c axes remain undistorted. With the addition of $\text{ZnTPY}:\text{SnI}_2$ heterogeneous nuclei, the quasi-cubic 2D/3D Sn-perovskite also exhibits the same crystal planes (Figure 3b). Interestingly, the addition of ZnTPY results in a stronger peak intensity for the $(10\bar{1})'$ plane compared to the $(20\bar{2})'$ facet, indicating a reduction in the periodicity of the $\text{PEA}_{0.15}\text{FA}_{0.8}\text{MA}_{0.05}\text{SnI}_3$ perovskite crystal along the b-axis, as shown in Figure 3c. This directly confirms that the introduction of $\text{ZnTPY}:\text{SnI}_2$ adducts leads to the formation of strong chelation between ZnTPY and Sn-perovskites, effectively preventing PEA^+ from rapidly cleaving crystals. In contrast, Figure 3d illustrates how the incorporation of the bulky PEA^+ molecule expands the 3D structure of the $\text{PEA}_{0.15}\text{FA}_{0.8}\text{MA}_{0.05}\text{SnI}_3$ crystal, disrupting continuity along the b-axis. Figure 3e demonstrates that the Sn-perovskite containing $\text{ZnTPY}:\text{SnI}_2$ displays improved crystallinity, supporting the claim that the PEA^+ -based perovskite has been effectively reconstructed. Additionally, XPS spectra were employed to investigate the effect of crystallinity optimization in Sn-perovskite crystals on changes in chemical composition (Figure S2). To estimate the oxidation state of Sn, we analyzed the characteristic peaks of Sn^{2+} and Sn^{4+} , which were split into two satellite signals, with binding energies of approximately 485.5 eV and 493.9 eV corresponding to the $3d_{5/2}$ and $3d_{3/2}$ states of Sn^{2+} , respectively, while 486.3 eV and 494.7 eV correspond to the $3d_{5/2}$ and $3d_{3/2}$ states of Sn^{4+} .⁵ It was observed that the

proportion of Sn^{4+} in the Sn-perovskite with the ZnTPY additive decreased from 14.38% to 9.57%. After peak integration, the proportion of Sn^{4+} in the ZnTPY-modified Sn-perovskite decreased from 14.38% to 9.57%. As a multidentate ligand, ZnTPY can chelate with Sn^{2+} to form a coordination complex, thereby inhibiting the oxidation of the Sn-perovskite film. This interaction improves the defect chemistry of the Sn-perovskite, leading to enhanced film quality. In sum, ZnTPY CONASHs can effectively retain the hydrophobic macroion PEA^+ within the crystal and maintain the high-quality quasi-cubic 2D/3D structure of tin perovskite through strong interactions with SnI_2 .

The alteration in crystal structure upon the inclusion of ZnTPY: SnI_2 heterogeneous nuclei was further validated through analyses using UV-vis absorbance spectroscopy and scanning electron microscopy (SEM). As presented in Figure 3f, the enhanced band-edge absorption of Sn-perovskite crystals within the wavelength range of 310-530 nm signifies improved crystallinity and orientation of Sn-perovskites⁴¹ that have been treated with ZnTPY: SnI_2 adducts. Moreover, this observation reflects the suppression of the formation of the 2D less-layered perovskite architecture.⁴² Thus, as demonstrated in the SEM image, the growth of Sn-perovskites with b-axis orientation promotes the formation of compact and smooth films (Figure 3g). In contrast, bare $\text{PEA}_{0.15}\text{FA}_{0.8}\text{MA}_{0.05}\text{SnI}_3$ films exhibit significant roughness, characterized by pinholes and voids resulting from uncontrolled crystal growth (Figure 3h). The enhanced morphology of the Sn-perovskite film, attributed to the presence of ZnTPY: SnI_2 heterogeneous nuclei, can be further elucidated by the uncoordinated TPY sites of ZnTPY CONASHs in the perovskite precursor solution. These TPY-terminated groups promote chelation with SnI_2 , leading to the formation of $[(\text{SnI}_{6-x})^4\text{-ZnTPY}]$ heterogeneous nuclei with low activation energies, thereby enhancing intuitive morphological optimization.

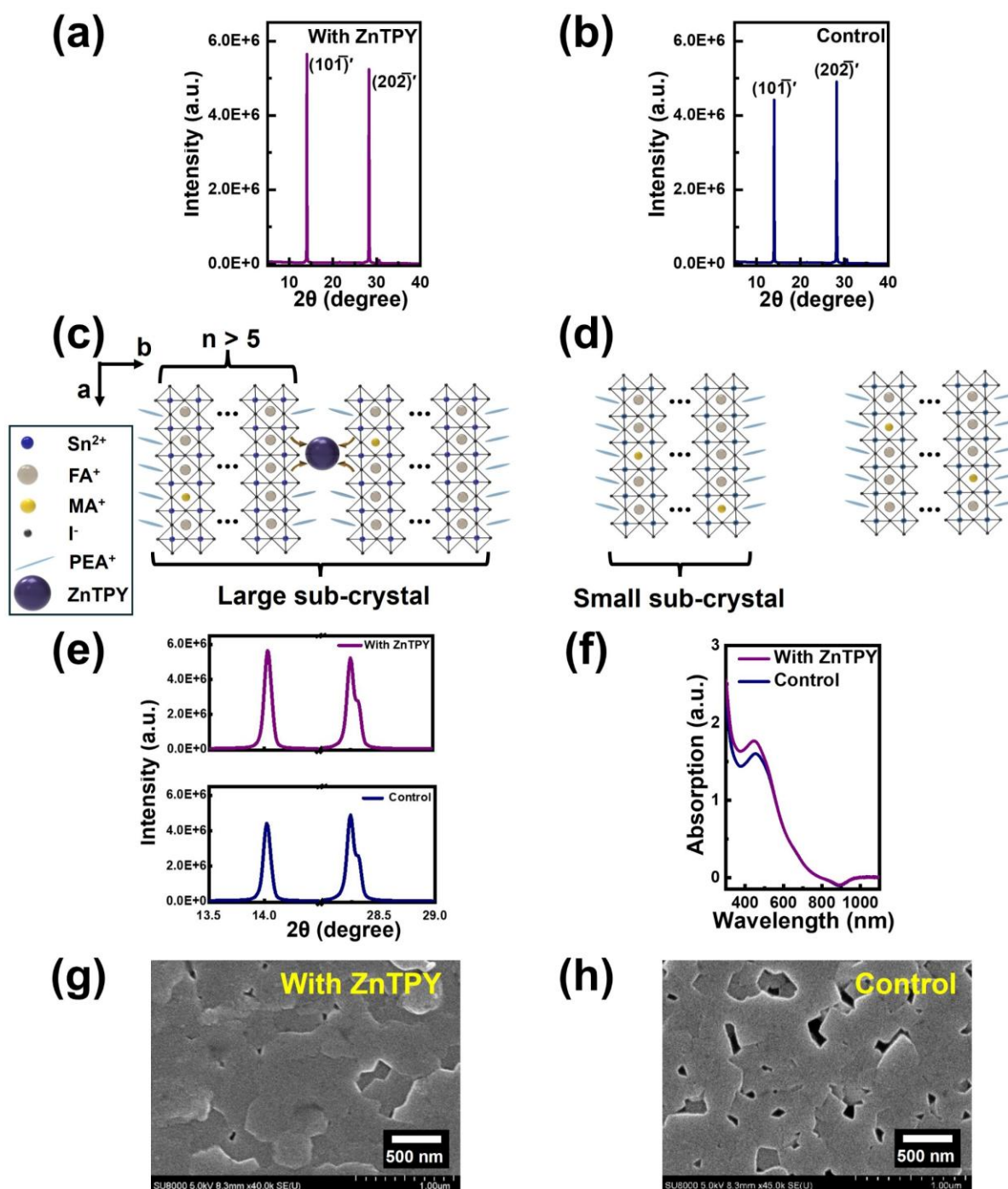


Figure 3. XRD patterns of $\text{PEA}_{0.15}\text{FA}_{0.8}\text{MA}_{0.05}\text{SnI}_3$ films: (a) with and (b) without ZnTPY CONASHs. (c) Schematic structure of ZnTPY-based $\text{PEA}_{0.15}\text{FA}_{0.8}\text{MA}_{0.05}\text{SnI}_3$ crystal and (d) bare $\text{PEA}_{0.15}\text{FA}_{0.8}\text{MA}_{0.05}\text{SnI}_3$ crystal. (e) Enlarged XRD peaks for the $(10\bar{1})'$ and $(20\bar{2})'$ planes. (f) Absorption spectra of Sn-perovskite films with and without ZnTPY. SEM images of Sn-perovskite films: (g) with ZnTPY additives and (h) without ZnTPY.

Photovoltaic performance

To evaluate the impact of crystallinity and morphological optimization on photovoltaic performance, we examined ZnTPY-incorporated perovskite sensitizers in Sn-PSCs with an architecture of ITO/poly(3,4-ethylenedioxythiophene):polystyrene sulfonate (PEDOT:PSS)/perovskite/indene-C₆₀ bisadduct (ICBA)/bathocuproine (BCP)/Ag, as schematically depicted in Figure 4a. In the device structure, PEDOT:PSS, ICBA, and BCP serve as the hole transporter, electron transporter, and hole-blocking layer, respectively. These thin films play a crucial role in the dissociation of excitons within the Sn-perovskite and enhance the transport of the resulting free charge carriers, ultimately mitigating electron-hole recombination in PSCs. Figure 4b presents the current density-voltage (J - V) characteristics of Sn-PSCs both without and with ZnTPY CONASHs, measured under simulated AM 1.5G illumination at the intensity of 100 mW/cm². The comprehensive J - V parameters are outlined in Table 1. The incorporation of ZnTPY leads to the formation of highly crystalline and smooth films, resulting in the highest PCE observed. The best PCE achieved with the incorporation of ZnTPY as additives in the perovskite layer is 11.59%, accompanied by a short-circuit current density (J_{sc}) of 19.06 mA/cm², an open-circuit voltage (V_{oc}) of 0.842 V, and a fill factor (FF) of 72.19%. These values surpass those of the control PSC device, which exhibited a PCE of 9.14%, a J_{sc} of 16.25 mA/cm², a V_{oc} of 0.807 V, and an FF of 69.70%, implying that the ZnTPY CONASH is an ideal additive for Sn-PSCs. The external quantum efficiency (EQE) spectrum allows for an analysis of the details behind the enhancement of J_{sc} , as shown in Figure 4c. The findings indicate that incorporating ZnTPY enhances photocurrent across the 300-850 nm range, effectively covering the entire visible spectrum. This advancement is primarily attributed to high crystallinity, compact morphology, and defect suppression. The reduction of defects (vacancies) helps mitigate hysteresis resulting from the polarization of the perovskite layers caused by the migration of iodide ions.⁴³ Hence, in Sn-PSCs constructed with ZnTPY CONASHs, a reduced J - V hysteresis is observed across various scanning directions

(Figure 4b). Moreover, we noted that the ZnTPY-planted Sn-PSCs displayed a statistically higher average PCE of $10.95 \pm 0.40\%$ with a narrower distribution compared to the control device, indicating reproducible superior performance, as illustrated in Figure S3 (detailed parameters) and summarized in Table 1 (PCE values).

Additionally, the ZnTPY-containing tin perovskite, which already incorporates hydrophobic PEA⁺ macromolecular, exhibits more complete crystallization compared to the pristine PEA_{0.15}FA_{0.8}MA_{0.05}SnI₃ perovskite. This modification is anticipated to enhance its resistance to the adhesion of water and oxygen, thereby increasing stability. **We thus assessed the long-term operational stability of Sn-PSCs with device encapsulation, comparing those with and without ZnTPY CONASHs by monitoring the maximum power point output, as described in Figure 4d. After 180 hours, the PCE of the reference cell decreased to below 40% of its original value, whereas the ZnTPY-based Sn-PSC maintained approximately 60% of its initial PCE after ~300 hours. This verifies that the ZnTPY CONASH also plays a beneficial role in enhancing the stability of the Sn-PSC.**

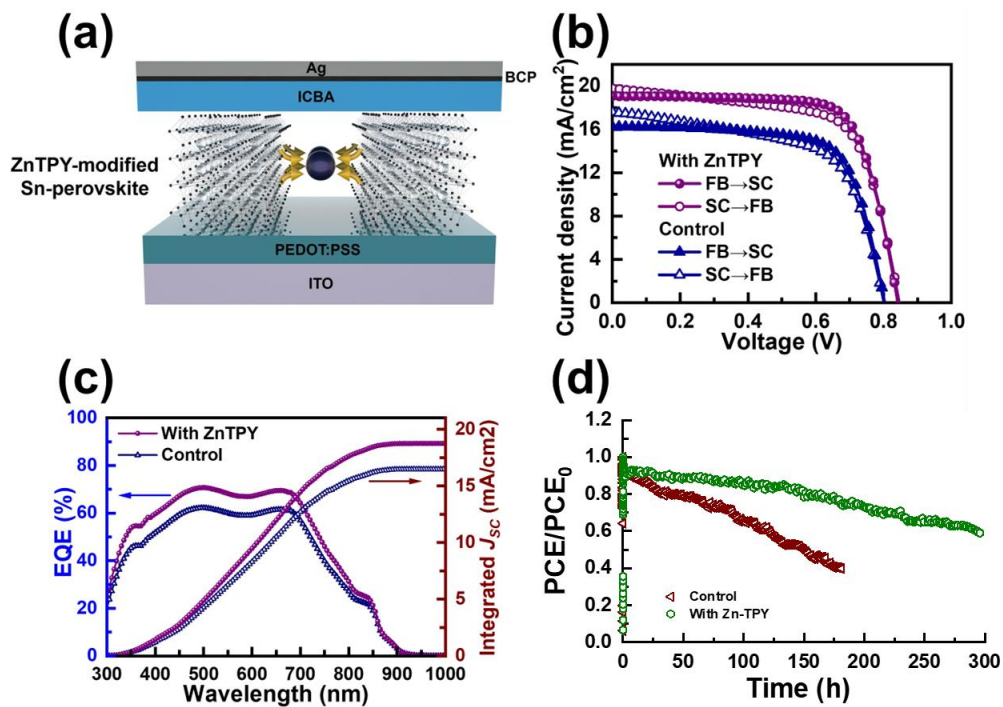


Figure 4. (a) Schematic representation of Sn-PSC device architecture, incorporating ZnTPY CONASHs as heterogeneous nucleation sites. (b) Reverse (FB→SC) and forward (SC→FB) J - V characteristics were measured under AM 1.5G illumination (100 mW cm^{-2}) for Sn-PSCs with and without the inclusion of the ZnTPY complex. (c) EQE spectrum and corresponding integrated J_{sc} curve of the highest-performing Sn-PSCs with and without insertion of ZnTPY CONASH. (d) Operational stability of Sn-PSCs with and without integration of ZnTPY evaluated at the maximum power point tracking (MPPT) with encapsulated devices under ambient air condition at 30-40 % relative humidity (RH).

Table 1. The summarized parameters of Sn-PSCs with and without ZnTPY CONASHs were measured under simulated AM 1.5G illumination at 100 mW cm^{-2} . The average values, along with the standard deviations (shown in brackets), were statistically calculated from data collected from 21 devices across 4 distinct batches.

Devices	J_{sc} (mA cm^{-2})	V_{oc} (V)	FF (%)	PCE (%)
With ZnTPY (FB→SC)	19.06	0.842	72.19	11.59 (10.95 ± 0.40)
With ZnTPY (SC→FB)	19.83	0.848	66.70	11.21
Control (FB→SC)	16.25	0.807	69.70	9.14 (8.51 ± 0.65)
Control (SC→FB)	17.68	0.801	61.12	8.66

Photodynamic analysis

Next, we investigated the correlation between enhanced photovoltaic performance and improved crystallinity of Sn-perovskite by analyzing photodynamic behaviors. Steady-state photoluminescence (PL) measurements revealed that perovskite films without any transport layers do not exhibit quenching, instead, only charge-carrier recombination is observed. Thus, the intensity of recombination is directly related to the quantity of photogenerated carriers generated inside the perovskite photoabsorber.⁴⁴ As illustrated in Figure 5a, the PL intensity of the ZnTPY-doped perovskite film is significantly higher than that of the bare Sn-perovskite, confirming that the introduction of ZnTPY CONASHs into the $\text{PEA}_{0.15}\text{FA}_{0.8}\text{MA}_{0.05}\text{SnI}_3$ perovskite enhances photocurrent generation. Typically, perovskites with better crystallinity and fewer defects exhibit an increase in photocurrent.⁴⁵ Therefore, the PL results demonstrate a trend that aligns with the results presented in Figure 3, indicating that ZnTPY CONASHs can enhance the generation of photocarriers by improving the crystallinity of the Sn-perovskite, ultimately leading to enhanced solar cell performance. For a more comprehensive analysis, the dynamics of photogenerated carriers within the tin perovskite can be assessed using time-resolved PL (TRPL) decay curves, as seen in Figure 5b. The TRPL analysis revealed a biexponential decay in the recombination dynamics, with each curve being deconvoluted into two stages characterized by distinct lifetimes. The inset table of Figure 5b lists the TRPL lifetimes, with τ_1 and τ_2 representing the fast and slow decay lifetimes of photocarriers following prolonged excitation, where τ_1 is associated with surface recombination and τ_2 corresponds to recombination within the interior of the pristine perovskite.⁴⁶ Clearly, the introduction of CONASHs into Sn-perovskite films yielded longer τ_1 (3.42 ns) and τ_2 (10.18 ns) values compared to bare films ($\tau_1 = 2.01$ ns and $\tau_2 = 4.52$ ns), indicating that charge-carrier recombination is taking place not only at the crystal surface but also within its interior. This implies that ZnTPY enhances the morphology of Sn-perovskite from the interior outward, thereby thoroughly improving the generation of photocurrent. In addition to investigating the

photodynamics of the perovskite film, we further examined the impact of ZnTPY CONASHs on enhancing Sn-PSC device performance. We applied laser pulses to modulate the V_{oc} and further measured the decay of transient photovoltage (TPV) signals to conduct device-level photodynamic analysis. Figure 5c illustrates that the charge-recombination lifetime decreased from 10.34 μs in the ZnTPY CONASH-treated PSC to 7.80 μs in the reference cell. The longer carrier recombination lifetime observed in the PSC containing CONASHs suggests that the chelation between the terminal TPY groups of fragmented ZnTPY and defective perovskite crystals mitigates surface defects, thereby decreasing trap-assisted recombination.^{47,48}

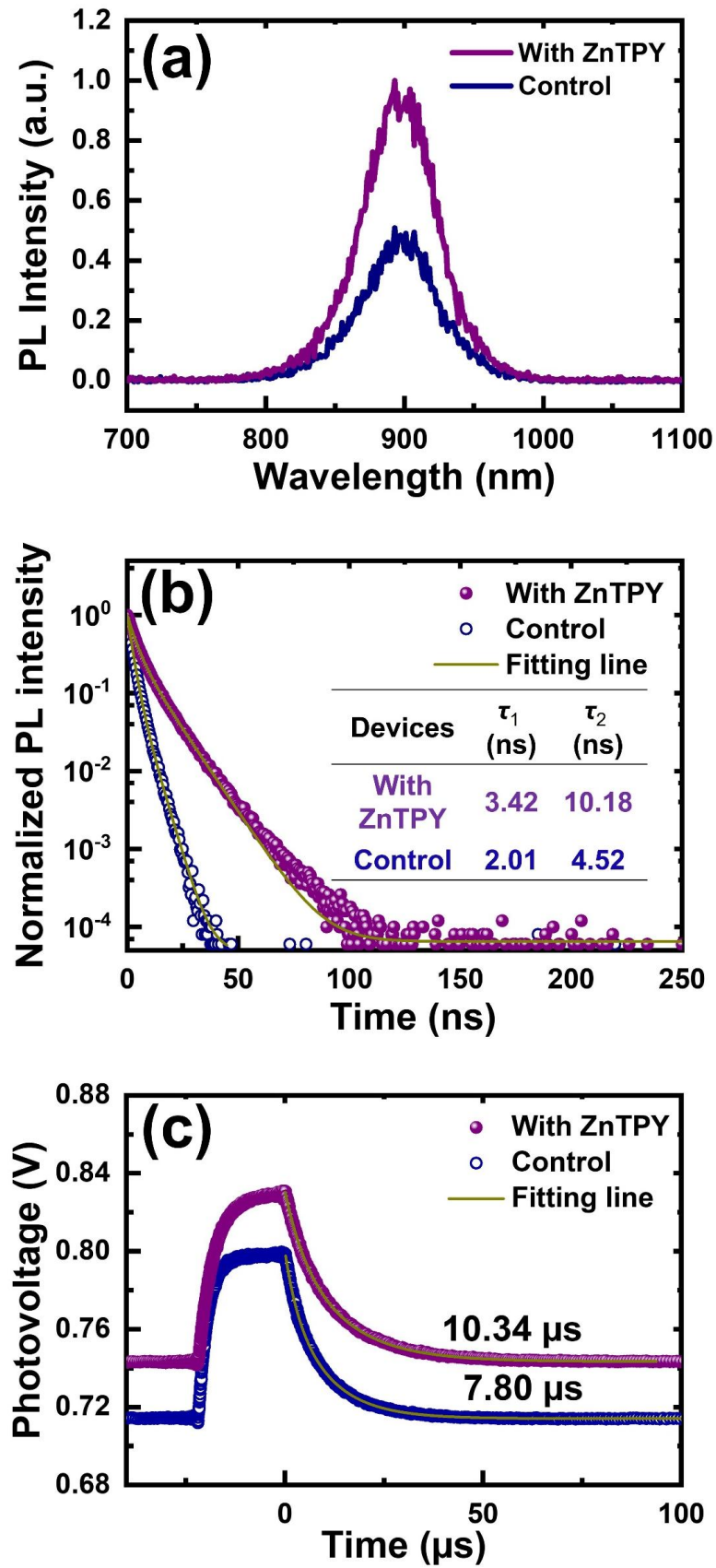


Figure 5. (a) Steady-state PL, (b) TRPL and (c) TPV decay curves of Sn-PSCs with and without ZnTPY additive.

Conclusion

In summary, this study demonstrates that ZnTPY CONASH is a promising additive for the formation of ZnTPY:SnI₂ heterogeneous nuclei, effectively repairing quasi-cubic 2D/3D Sn-perovskite crystals affected by the insertion of bulky PEA⁺ molecules. The experimental results indicate a significant reduction in the 2D phase, resulting in an overall enhancement of crystallinity. The incorporation of ZnTPY-modified tin perovskite as the photoactive layer in PSC devices leads to simultaneous improvements in both PCE and operational stability. Thus, π -conjugated CONASHs offer an innovative crystallization strategy for Sn-perovskites and demonstrate broad applicability for enhancing the performance of other environmentally friendly PSCs.

ASSOCIATED CONTENT

Supporting Information

Electronic supplementary information (ESI) available: Experimental section, additional figures. This material is available free of charge via the Internet.

AUTHOR INFORMATION

Corresponding authors

*Email: KHADKA.B.Dhruba@nims.go.jp (D.B.K.)

*Email: ycwang@mail.nsysu.edu.tw (Y.-C.W.)

ORCID

Dhruba B. Khadka: 0000-0001-9134-3890

Masatoshi Yanagida: 0000-0002-8065-7875

Hiroshi Nishihara: 0000-0002-6568-5640

Kazuhito Tsukagoshi: 0000-0001-9710-2692

Yasuhiro Shirai: 0000-0003-2164-5468

Ying-Chiao Wang: 0000-0002-6459-0770

Conflicts of Interest

The authors declare no competing financial interest.

Acknowledgments

This work was supported by The Hitachi Global Foundation, Kurata grant #1572. The authors are grateful to Yamaguchi Kazuo-San (XPS) and Takahashi Hiromi (XRD) in the battery research platform for the technical support for respective measurement and analysis. Y.-C.W.

acknowledges the financial support from the National Science and Technology Council (NSTC), Taiwan, R.O.C. (Grant No. NSTC 113-2221-E-110-005- and NSTC 112-2222-E-110-004-). This work was also supported by the Taiwan Comprehensive University System (TCUS). And Y.-C.W. thanks the Yushan Fellow Program by the Ministry of Education (MOE), Taiwan for the financial support. Y.-C.W. also acknowledges the Photovoltaic Materials Group at the National Institute for Materials Science for hosting him as a short-term visiting scholar. The authors are deeply thankful to Prof. Kenjiro Miyano for his insightful comments and constructive suggestions in this work.

References

1. Park, J.; Kim, J.; Yun, H.-S.; Paik, M. J.; Noh, E.; Mun, H. J.; Kim, M. G.; Shin, T. J.; Seok, S. I. Controlled growth of perovskite layers with volatile alkylammonium chlorides. *Nature* **2023**, *616*, 724-730.
2. Khadka, D. B.; Shirai, Y.; Yanagida, M.; Ryan, J. W.; Song, Z.; Barker, B. G.; Dhakal, T. P.; Miyano, K. Advancing efficiency and stability of lead, tin, and lead/tin perovskite solar cells: strategies and perspectives. *Sol. RRL* **2023**, *7*, 2300535.
3. Chen, H.; Liu, C.; Xu, J.; Maxwell, A.; Zhou, W.; Yang, Y.; Zhou, Q.; Bati, A. S. R.; Wan, H.; Wang, Z.; Zeng, L.; Wang, J.; Serles, P.; Liu, Y.; Teale, S.; Liu, Y.; Saidaminov, M. I.; Li, M.; Rolston, N.; Hoogland, S.; Filleter, T.; Kanatzidis, M. G.; Chen, B.; Ning, Z.; Sargent, E. H. Improved charge extraction in inverted perovskite solar cells with dual-site-binding ligands. *Science* **2024**, *384*, 189-193.
4. Zheng, Y.; Li, Y.; Zhuang, R.; Wu, X.; Tian, C.; Sun, A.; Chen, C.; Guo, Y.; Hua, Y.; Meng, K.; Wu, K.; Chen, C.-C. Towards 26% efficiency in inverted perovskite solar cells via interfacial flipped band bending and suppressed deep-level traps. *Energy Environ. Sci.* **2024**, *17*, 1153-1162.
5. Khadka, D. B.; Shirai, Y.; Yanagida, M.; Tadano, T.; Miyano, K. Alleviating defect and oxidation in tin perovskite solar cells using a bidentate ligand. *Chem. Mater.* **2023**, *35*, 4250-4258.
6. Chen, C.-H.; Cheng, S.-N.; Hu, F.; Su, Z.-H.; Wang, K.-L.; Cheng, L.; Chen, J.; Shi, Y.-R.; Xia, Y.; Teng, T.-Y.; Gao, X.-Y.; Yavuz, I.; Lou, Y.-H.; Wang, Z.-K. Lead isolation and capture in perovskite photovoltaics toward eco-friendly commercialization. *Adv. Mater.* **2024**, *36*, 2403038.

7. Cortecchia, D.; Dewi, H. A.; Yin, J.; Bruno, A.; Chen, S.; Baikie, T.; Boix, P. P.; Grätzel, M.; Mhaisalkar, S.; Soci, C.; Mathews, N. Lead-free MA₂CuCl_xBr_{4-x} hybrid perovskites. *Inorg. Chem.* **2016**, *55*, 1044-1052.
8. Wu, C.; Zhang, Q.; Liu, G.; Zhang, Z.; Wang, D.; Qu, B.; Chen, Z.; Xiao, L. From Pb to Bi: A promising family of Pb-free optoelectronic materials and devices. *Adv. Energy Mater.* **2020**, *10*, 1902496.
9. Zhou, X.; Peng, W.; Liu, Z.; Zhang, Y.; Zhang, L.; Zhang, M.; Liu, C.; Yan, L.; Wang, X.; Xu, B. Additive engineering with 2,8-dibromo-dibenzothiophene-S,S-dioxide enabled tin-based perovskite solar cells with 14.98% power conversion efficiency. *Energy Environ. Sci.* **2024**, *17*, 2837-2844.
10. Sun, C.; Yang, P.; Nan, Z.; Tian, C.; Cai, Y.; Chen, J.; Qi, F.; Tian, H.; Xie, L.; Meng, L.; Wei, Z. Well-defined fullerene bisadducts enable high-performance tin-based perovskite solar cells. *Adv. Mater.* **2023**, *35*, 2205603.
11. Wang, S.; Bidinakis, K.; Haese, C.; Hasenburger, F. H.; Yildiz, O.; Ling, Z.; Frisch, S.; Kivala, M.; Graf, R.; Blom, P. W. M.; Weber, S. A. L.; Pisula, W.; Marszalek, T. Modification of two-dimensional tin-based perovskites by pentanoic acid for improved performance of field-effect transistors. *Small.* **2023**, *19*, 2207426.
12. Zeng, G.; Pu, D.; Huang, L.; Guan, H.; Zhou, S.; Zhou, J.; Shen, W.; Li, G.; Fang, G.; Ke, W. Enhancing the performance of tin-based perovskite solar cells through solvent purification of tin iodide. *J. Mater. Chem. A.* **2023**, *11*, 11245-11253.
13. Song, D.; Li, H.; Xu, Y.; Yu, Q. Amplifying hole extraction characteristics of PEDOT:PSS via post-treatment with aromatic diammonium acetates for tin perovskite solar cells. *ACS Energy Lett.* **2023**, *8*, 3280-3287.
14. Zhao, J.; Zhang, Z.; Li, G.; Aldamasy, M. H.; Li, M.; Abate, A. Dimensional tuning in lead-free tin halide perovskite for solar cells. *Adv. Energy Mater.* **2023**, *13*, 2204233.

15. Macdonald, T. J.; Lanzetta, L.; Liang, X.; Ding, D.; Haque, S. A. Engineering stable lead-free tin halide perovskite solar cells: Lessons from materials chemistry. *Adv. Mater.* **2023**, *35*, 2206684.
16. Wang, S.; Yao, H.; Zhu, W.; Wu, C.; Tang, Z.; Liu, J.; Ding, L.; Hao, F. Stabilization of perovskite lattice and suppression of Sn²⁺/Sn⁴⁺ oxidation via formamidine acetate for high efficiency tin perovskite solar cells. *Adv. Funct. Mater.* **2023**, *33*, 2215041.
17. Wang, H.; He, J.; Xiang, H.; Ran, R.; Zhou, W.; Wang, W.; Shao, Z. Additive engineering for mixed lead-tin narrow-band-gap perovskite solar cells: Recent advances and perspectives. *Energy Fuels.* **2023**, *37*, 6401-6423.
18. Zhang, W.; Yuan, H.; Li, X.; Guo, X.; Lu, C.; Liu, A.; Yang, H.; Xu, L.; Shi, X.; Fang, Z.; Yang, H.; Cheng, Y.; Fang, J. Component distribution regulation in Sn-Pb perovskite solar cells through selective molecular interaction. *Adv. Mater.* **2023**, *35*, 2303674.
19. Wang, L.; Miao, Q.; Wang, D.; Chen, M.; Bi, H.; Liu, J.; Baranwal, A. K.; Kapil, G.; Sanehira, Y.; Kitamura, T.; Ma, T.; Zhang, Z.; Shen, Q.; Hayase, S. 14.31 % Power conversion efficiency of Sn-Based perovskite solar cells via efficient reduction of Sn⁴⁺. *Angew. Chem. Int. Ed.* **2023**, *62*, e202307228.
20. Zhao, Z.; Gu, F.; Li, Y.; Sun, W.; Ye, S.; Rao, H.; Liu, Z.; Bian, Z.; Huang, C. Mixed-organic-cation tin iodide for lead-free perovskite solar cells with an efficiency of 8.12%. *Adv. Sci.* **2017**, *4*, 1700204.
21. Cao, K.; Cheng, Y.; Zuo, W.; Cai, B.; Wu, Y.; Zhu, J.; Zhu, Y.; Ning, H.; Shen, Y.; Shen, W.; Liu, L.; Chen, S. Ionic compensation for defect reduction and enhanced performance of tin-based perovskite solar cells. *J. Power Sources* **2023**, *558*, 232595.
22. Noel, N. K.; Stranks, S. D.; Abate, A.; Wehrenfennig, C.; Guarnera, S.; Haghighirad, A.-A.; Sadhanala, A.; Eperon, G. E.; Pathak, S. K.; Johnston, M. B.; Petrozza, A.; Herz, L. M.;

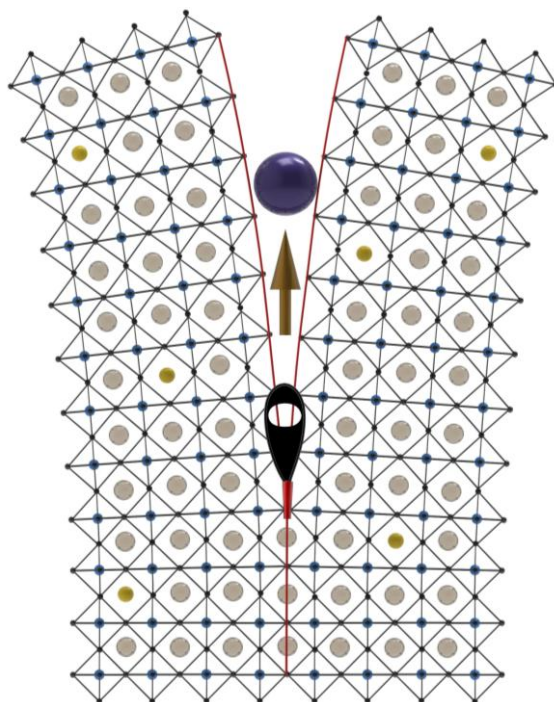
- Snaith, H. J. Lead-free organic-inorganic tin halide perovskites for photovoltaic applications. *Energy Environ. Sci.* **2014**, *7*, 3061-3068.
23. Hao, F.; Stoumpos, C. C.; Cao, D. H.; Chang, R. P. H.; Kanatzidis, M. G. Lead-free solid-state organic-inorganic halide perovskite solar cells. *Nat. Photonics* **2014**, *8*, 489-494.
24. Cao, D. H.; Stoumpos, C. C.; Yokoyama, T.; Logsdon, J. L.; Song, T.-B.; Farha, O. K.; Wasielewski, M. R.; Hupp, J. T.; Kanatzidis, M. G. Thin films and solar cells based on semiconducting two-dimensional Ruddlesden-Popper $(\text{CH}_3(\text{CH}_2)_3\text{NH}_3)_2(\text{CH}_3\text{NH}_3)_{n-1}\text{Sn}_n\text{I}_{3n+1}$ perovskites. *ACS Energy Lett.* **2017**, *2*, 982-990.
25. Diau, E. W.-G.; Jokar, E.; Rameez, M. Strategies to improve performance and stability for tin-based perovskite solar cells. *ACS Energy Lett.* **2019**, *4*, 1930-1937.
26. Shi, T.; Zhang, H.-S.; Meng, W.; Teng, Q.; Liu, M.; Yang, X.; Yan, Y.; Yip, H.-L.; Zhao, Y.-J. Effects of organic cations on the defect physics of tin halide perovskites. *J. Mater. Chem. A*, **2017**, *5*, 15124-15129.
27. Li, B.; Chang, B.; Pan, L.; Li, Z.; Fu, L.; He, Z.; Yin, L. Tin-based defects and passivation strategies in tin-related perovskite solar cells. *ACS Energy Lett.* **2020**, *5*, 3752-3772.
28. Yang, W.-F.; Igbari, F.; Lou, Y.-H.; Wang, Z.-K.; Liao, L.-S. Tin halide perovskites: Progress and challenges. *Adv. Energy Mater.* **2020**, *10*, 1902584.
29. Zhang, Z.; Su, Z.; Li, G.; Li, J.; Aldamasy, M. H.; Wu, J.; Wang, C.; Li, Z.; Gao, X.; Li, M.; Abate, A. Improved air stability of tin halide perovskite solar cells by an N-type active moisture barrier. *Adv. Funct. Mater.* **2024**, *34*, 2306458.
30. Jokar, E.; Chien, C.-H.; Fathi, A.; Rameez, M.; Chang, Y.-H.; Diau, E. W.-G. Slow surface passivation and crystal relaxation with additives to improve device performance and durability for tin-based perovskite solar cells. *Energy Environ. Sci.* **2018**, *11*, 2353-2362.

31. Yao, H.; Zhu, W.; Hu, J.; Wu, C.; Wang, S.; Zhao, X.; Niu, X.; Ding, L.; Hao, F. Halogen engineering of 2D/3D tin halide perovskite for enhanced structural stability. *Chem. Eng. J.* **2023**, *455*, 140862.
32. Lee, D. S.; Yun, J. S.; Kim, J.; Soufiani, A. M.; Chen, S.; Cho, Y.; Deng, X.; Seidel, J.; Lim, S.; Huang, S.; Ho-Baillie, A. W. Y. Passivation of grain boundaries by phenethylammonium in formamidinium-methylammonium lead halide perovskite solar cells. *ACS Energy Lett.* **2018**, *3*, 647-654.
33. Liao, Y.; Liu, H.; Zhou, W.; Yang, D.; Shang, Y.; Shi, Z.; Li, B.; Jiang, X.; Zhang, L.; Quan, L. N.; Quintero-Bermudez, R.; Sutherland, B. R.; Mi, Q.; Sargent, E. H.; Ning, Z. Highly oriented low-dimensional tin halide perovskites with enhanced stability and photovoltaic performance. *J. Am. Chem. Soc.* **2017**, *139*, 6693-6699.
34. Wang, Y.-C.; Chiang, C.-H.; Su, C.-J.; Chang, J.-W.; Lin, C.-Y.; Wei, C.-C.; Huang, S.-K.; Maeda, H.; Jian, W.-B.; Jeng, U.-S.; Tsukagoshi, K.; Chen, C.-W.; Nishihara, H. Terpyridine-zinc(ii) coordination nanosheets as modulators of perovskite crystallization to enhance solar cell efficiency. *J. Mater. Chem. A.* **2023**, *11*, 7077-7084.
35. Tsukamoto, T.; Takada, K.; Sakamoto, R.; Matsuoka, R.; Toyoda, R.; Maeda, H.; Yagi, T.; Nishikawa, M.; Shinjo, N.; Amano, S.; Iokawa, T.; Ishibashi, N.; Oi, T.; Kanayama, K.; Kinugawa, R.; Koda, Y.; Komura, T.; Nakajima, S.; Fukuyama, R.; Fuse, N.; Mizui, M.; Miyasaki, M.; Yamashita, Y.; Yamada, K.; Zhang, W.; Han, R.; Liu, W.; Tsubomura, T.; Nishihara, H. Coordination nanosheets based on terpyridine-zinc(II) complexes: As photoactive host materials. *J. Am. Chem. Soc.* **2017**, *139*, 5359-5366.
36. Mitzi, D. B. Templating and structural engineering in organic-inorganic perovskites, *J. Chem. Soc., Dalton Trans.* **2001**, 1-12. (Plz check it)

37. Cheng, Z.; Lin, J. Layered organic-inorganic hybrid perovskites: structure, optical properties, film preparation, patterning and templating engineering, *CrystEngComm*, **2010**, *12*, 2646.
38. Shimada, K.; Maruyama, S.; Miyadera, T.; Kaminaga, K.; Matsumoto, Y. Reaction dynamics of $C(NH_2)_3SnI_3$ formation from vacuum-deposited $C(NH_2)_3I$ and SnI_2 bilayer thin films investigated by in situ infrared multiple-angle incidence-resolved spectroscopy. *ACS Appl. Mater. Interfaces* **2023**, *15*, 45411-45417.
39. Rao, H.; Su, Y.; Liu, G.; Zhou, H.; Yang, J.; Sheng, W.; Zhong, Y.; Tan, L.; Chen, Y. Monodisperse adducts-induced homogeneous nucleation towards high-quality tin-based perovskite film. *Angew. Chem. Int. Ed.* **2023**, *62*, e202306712.
40. Cho, S. W.; Pandey, P.; Park, J.; Lee, T.-W.; Ahn, H.; Choi, H.; Kang, D.-W. Phenylethylammonium-formamidinium-methylammonium quasi-2D/3D tin wide-bandgap perovskite solar cell with improved efficiency and stability. *Chem. Eng. J.* **2022**, *446*, 137388.
41. Chang, B.; Li, B.; Wang, Z.; Li, H.; Wang, L.; Pan, L.; Li, Z.; Yin, L. Efficient bulk defect suppression strategy in $FASnI_3$ perovskite for photovoltaic performance enhancement. *Adv. Funct. Mater.* **2022**, *32*, 2107710.
42. Yu, B.-B.; Wu, Y.; Wang, H.; Hu, X.; Zhang, Z.; Wang, S.; Chen, G. Y.; Qin, Q.; Huang, L.-B. High-efficiency tin perovskite solar cells by the dual functions of reduced voltage loss and crystal regulation. *Mater. Des.* **2023**, *228*, 111850.
43. Meloni, S.; Moehl, T.; Tress, W.; Franckevičius, M.; Saliba, M.; Lee, Y. H.; Gao, P.; Nazeeruddin, M. K.; Zakeeruddin, S. M.; Rothlisberger, U.; Grätzel, M. Ionic polarization-induced current-voltage hysteresis in $CH_3NH_3PbX_3$ perovskite solar cells *Nat. Commun.* **2016**, *7*, 10334.

44. Wang, Y.-C.; Chang, J.; Zhu, L.; Li, X.; Song, C.; Fang, J. Electron-transport-layer-assisted crystallization of perovskite films for high-efficiency planar heterojunction solar cells. *Adv. Funct. Mater.* **2018**, *28*, 1706317.
45. Chen, J.; Zhu, G.-P.; Li, X.; Lou, Y.-H.; Dong, C.; Wang, K.-L.; Yuan, S.; Chen, C.-H.; Shi, Y.-R.; Wang, T.; Wang, Z.-K. Visualizing the surface photocurrent distribution in perovskite photovoltaics. *Small* **2022**, *18*, 2201930.
46. Jia, P.; Qin, L.; Zhao, D.; Tang, Y.; Song, B.; Guo, J.; Li, X.; Li, L.; Cui, Q.; Hu, Y.; Lou, Z.; Teng, F.; Hou, Y. The trapped charges at grain boundaries in perovskite solar cells. *Adv. Funct. Mater.* **2021**, *31*, 2107125.
47. Yang, S.; Chen, S.; Mosconi, E.; Fang, Y.; Xiao, X.; Wang, C.; Zhou, Y.; Yu, Z.; Zhao, J.; Gao, Y.; Angelis, F. D.; Huang, J. Stabilizing halide perovskite surfaces for solar cell operation with wide-bandgap lead oxysalts. *Science* **2019**, *365*, 473-478.
48. Khadka, D. B.; Shirai, Y.; Yanagida, M.; Ota, H.; Lyalin, A.; Taketsugu, T.; Miyano, K. Defect passivation in methylammonium/bromine free inverted perovskite solar cells using charge-modulated molecular bonding. *Nat. Commun.* **2024**, *15*, 882.

Table of Contents



π -conjugated terpyridine-zinc(II) (ZnTPY) coordination nanosheets (CONASHs) can serve as repair agents for 2D/3D tin-based perovskites, functioning like a zipper to optimize both crystallinity and orientation. When applied in solar cells, this approach enhances both the power conversion efficiency and operational stability of the devices. Thus, this strategy has the potential to improve the performance of other environmentally friendly perovskite solar cells in the future.